Proceedings of ALGORITMY 2012
pp. 427 - 437

APPLICATION OF A DEGENERATE DIFFUSION METHOD IN 3D MEDICAL IMAGE PROCESSING

RADEK MÁCA* AND MICHAL BENEŠ†

Abstract. In this contribution, we present the application of the level set formulation of the geodesic active contours model and its 3D semi-implicit complementary volume discretization to the segmentation of 2D+t cardiac MRI (CMR) data. The appropriate adujstment of algorithm parameters is explained. In particular, the algorithm is applied to the segmentation of the left and right heart ventricle from the time series of 2D+t cine CMR data.

Key words. cardiac MRI, co-volume method, image segmentation, level set method, PDE

AMS subject classifications. 35K60, 35K65, 65N06, 68U10

1. Heart ventricle segmentation. In this paper, we focus on the segmentation of the heart ventricles from cardiac magnetic resonance imaging (CMR) data. The CMR is a highly specialized imaging technique in the heart examination. In comparison with the magnetic resonance imaging (MRI) of other organs, the CMR has to take into account the motion of the heart, breathing motion and the blood flow in the heart cavities. The images are usually acquired over several cardiac cycles triggered by the patient's ECG (Electrocardiography). There are several cardiac MRI sequences used in the clinical practice. The image data we focus on are obtained by the Cine MRI referring to an examination of the heart kinematics. The heart is covered by 2D planes with the spatial resolution of about $2 \times 2 \times 10$mm. Therefore, the ventricles can be entirely covered by 8–12 slices. The planning of acquisition in short axis is presented in Fig. 1.1. The temporal resolution ranges between 20ms and 60ms, i.e. the cardiac cycle is usually covered by 15–50 time frames (see Fig. 1.2). For a detailed information about the MRI and the heart ventricle segmentation from the medical viewpoint see [3], [6].

In terms of the CMR data dimension, there are several possibilities of segmentation. The slices for each time frame can be either segmented as separate 2D images (see [1], [2], [10], [12], [16], [18], [21]) or merged into a 3D image [7]. As mentioned above, the resolution in the third dimension typically ranges between 8–12 which is much lower than in the other two. It is more convenient to segment the time evolution of each individual slice as a 3D (2D+t) image with the resolution in time between 15–50 (see [14]). Last, we could join all 2D slices in all time frames to produce a 4D (3D+t) image ([11], [17]). One of the first results dealing with the segmentation of 3D+t echocardiography images can be found in [25].

One of the drawbacks of 2D approach is the time discontinuity of the segmentation results which can be fixed using the 2D+t segmentation. Specifically, the 2D+t image

*Department of Mathematics, Faculty of Nuclear Sciences and Physical Engineering, Czech Technical University in Prague, Trojanova 13, Praha 2, 120 00, Czech Republic (radek.maca@fjfi.cvut.cz)

†Department of Mathematics, Faculty of Nuclear Sciences and Physical Engineering, Czech Technical University in Prague, Trojanova 13, Praha 2, 120 00, Czech Republic (michal.benes@fjfi.cvut.cz)

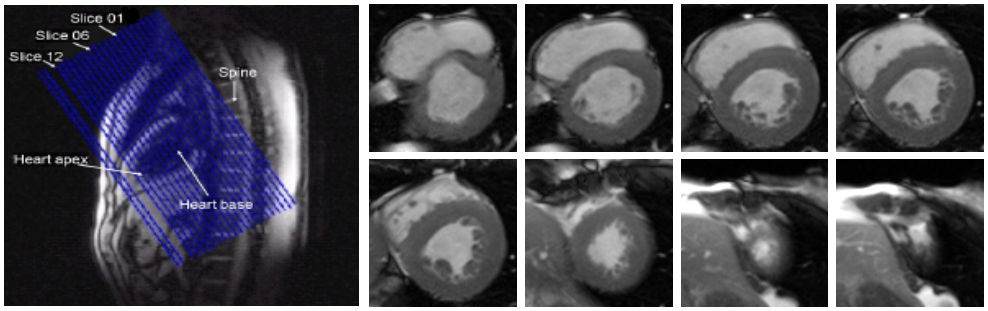

(a) (b)

Fig. 1.1: Example of data acquisition planning in short axis (a). The whole ventricle is covered by 12 slices denoted by S01–S12. In Figure (b), slices 01–05, 08 and 11–12 are depicted (from left to right).

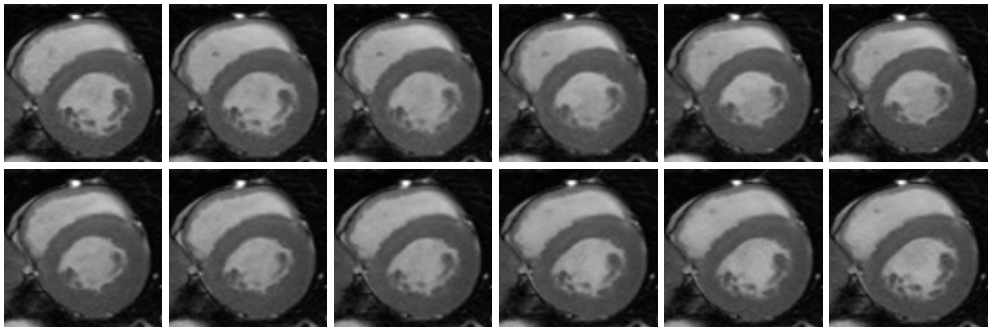

Fig. 1.2: A cardiac cycle is covered (for this patient) by 26 time frames (T01–T26). Even time frames (except for frame 26) for slice S03 are depicted.

is built of the time sequences of 2D images (see Fig. 1.2). This approach ensures the time continuity in the segmented data.

The main contribution of this paper is the segmentation algorithm based on the level set formulation of the geodesic active contours model and its 3D semi-implicit complementary volume discretization. The algorithm is tested on and applied to the segmentation of 2D+t CMR data.

2. Degenerate diffusion in image processing. In our case, the 3D or 2D+t CMR data are segmented by means of the surface $\Gamma(t) \subset \Omega$ in $\mathbb{R}^3$ propagating in the normal direction with velocity V. The velocity V at a surface point $\vec{x} \in \Gamma(t)$ is given by its (mean) curvature κ_Γ and external force as follows

$$V = -\kappa_\Gamma + F\,. \tag{2.1}$$

For the segmentation purposes, equation (2.1) can be modified by incorporating the influence of the processed signal (or its gradient) into the curvature and the force terms. The motion equation (2.1) can be treated by the level set method. In this

case, $\Gamma(t)$ is represented as a level set

$$\Gamma(t) = \{\vec{x} \in \Omega \,|\, u(t, \vec{x}) = 0\}\,, \tag{2.2}$$

where $u : [0, T] \times \Omega \to \mathbb{R}$. The variable t parameterizes the segmentation process and does not have the meaning of real time.

The evolution equation implicitly describing the motion of $\Gamma(t)$ given by (2.2) with velocity V in the outward normal direction is derived as follows.

Using the sign convention we can express the normal vector, the normal velocity and the mean curvature as

$$\vec{n} = \frac{\nabla u}{|\nabla u|}\,, \quad V = -\frac{\partial_t u}{|\nabla u|}\,, \quad \kappa_\Gamma = \nabla \cdot \vec{n} = \nabla \cdot \frac{\nabla u}{|\nabla u|}\,. \tag{2.3}$$

Substituting (2.3) to equation (2.1), we obtain the level set equation in the form

$$\partial_t u = |\nabla u|\, \nabla \cdot \frac{\nabla u}{|\nabla u|} - |\nabla u|\, F\,, \tag{2.4}$$

where we denote $\partial_t u := \partial u / \partial t$. This equation has been extensively studied and applied (see [8], [20], [26]). This experience suggests a ε-regularization [8] useful both for theory and numerical computation in the form:

$$\partial_t u = |\nabla u|_\varepsilon \nabla \cdot \frac{\nabla u}{|\nabla u|_\varepsilon} - |\nabla u|_\varepsilon F\,, \tag{2.5}$$

where

$$|\nabla u|_\varepsilon = \sqrt{\varepsilon^2 + |\nabla u|^2}\,, \quad \varepsilon > 0\,. \tag{2.6}$$

The known features of the level set equation based mainly on the controlled motion of isosurfaces of the solution naturally led to its use in the image processing (see [4], [13], [16], [23], [24], [26]).

In particular, the detection of image object edges is a one of tasks in image segmentation. Edges in the input image $I^0 : \Omega \to \{0, 1, 2 \ldots, I_{\max}\}$, represented by the matrix $n_x \times n_y \times n_z$, where the third direction corresponds to the time of the processed data

$$\Omega = (0, n_x/n) \times (0, n_y/n) \times (0, n_z/n)\,, \qquad n := \max\{n_x, n_y, n_z\}\,,$$

can be recognized by the magnitude of its spatial gradient. We use the following format of the CMR data size: $n_x \times n_y \times n_z \times n_s$, where n_s denotes number of slices. The level set equation operating in Ω can be modified as follows [5]

$$\partial_t u = |\nabla u|_\varepsilon \nabla \cdot \left(g\left(\left|\nabla G_\sigma * I^0\right|\right) \frac{\nabla u}{|\nabla u|_\varepsilon} \right) - g\left(\left|\nabla G_\sigma * I^0\right|\right) |\nabla u|_\varepsilon F\,, \tag{2.7}$$

where $g : \mathbb{R}_0^+ \to \mathbb{R}^+$ is a non-increasing function for which $g(0) = 1$ and $g(s) \to 0$ for $s \to +\infty$. This function was first used by P. Perona and J. Malik ([22] in 1987) to modify the heat equation into a nonlinear diffusion equation which maintains edges in an image. Consequently, the function g is called the Perona-Malik function. We

put $g(s) = 1/(1+\lambda s^2)$ with $\lambda \geq 0$. $G_\sigma \in \mathcal{C}^\infty(\mathbb{R}^3)$ is a smoothing kernel, e.g. the Gaussian with zero mean and variance σ^2

$$G_\sigma(\vec{x}) = \frac{1}{(2\pi)^{3/2}\,\sigma_x^3\sigma_y^3\sigma_z^3} \exp\left(-\frac{x^2}{2\sigma_x^2} - \frac{y^2}{2\sigma_y^2} - \frac{z^2}{2\sigma_z^2}\right), \tag{2.8}$$

which is used in pre-smoothing (denoising) of image gradients by the convolution

$$(\nabla G_\sigma * I^0)(\vec{y}) = \int_{\mathbb{R}^3} \bar{\nabla} G_\sigma(\vec{y}-\vec{x}) I^0(\vec{x})\,\mathrm{d}\vec{x}\,, \tag{2.9}$$

where $\bar{I}^0$ is the extension of I^0 to $\mathbb{R}^3$ by, e.g., mirroring, periodic prolongation or extension by zero. Let us note that equation (2.7) can be rewritten into the advection-diffusion form

$$\partial_t u = \underbrace{g^0 |\nabla u|_\varepsilon \nabla \cdot \left(\frac{\nabla u}{|\nabla u|_\varepsilon}\right)}_{(D)} + \underbrace{\nabla g^0 \cdot \nabla u}_{(A)} - \underbrace{g^0 |\nabla u|_\varepsilon F}_{(F)}\,. \tag{2.10}$$

For convenience, the abbreviation $g^0 = g(\left|\nabla G_\sigma * I^0\right|)$ is used. (D) in (2.10) denotes the diffusion term, (A) the advection term and (F) the external force term. The term g^0 is called the edge detector. The value of the edge detector is approximately equal to zero close to image edges (high gradients of input image). Consequently, the evolution of the segmentation function slows down in the neighbourhood of image edges. On the contrary, in parts of the image with constant intensity the edge detector equals one. The advection term attracts the segmentation function to the image edges.

2.1. Initial-boundary value problem. As a parabolic partial differential equation, (2.7) requires initial and boundary conditions. For this purpose, we define the signed distance function (SDF).

Let Γ_{in} be the interior of $\Gamma(t)$ and Γ_{out} be the exterior of $\Gamma(t)$. Consequently $\Gamma = \partial\Gamma_{\text{in}} = \partial\Gamma_{\text{out}}$, $\Gamma_{\text{in}} \cup \Gamma \cup \Gamma_{\text{out}} = \Omega$. Then the signed distance function (d_Γ) is given by

$$d_\Gamma(t,x) = \begin{cases} \operatorname{dist}(x,\Gamma(t)) & x \in \Gamma_{\text{out}}\,, \\ 0 & x \in \Gamma(t)\,, \\ -\operatorname{dist}(x,\Gamma(t)) & x \in \Gamma_{\text{in}}\,, \end{cases} \tag{2.11}$$

where $\operatorname{dist}(\vec{x},\Gamma(t)) = \min\{|\vec{x}-\vec{y}| \mid \vec{y} \in \Gamma(t)\}$.

The initial surface Γ_0 as the initial guess has to be placed inside the segmentation object – the left/right heart ventricle (see Fig. 2.1). Expansion of the initial surface requires velocity (2.1) to be positive. Positive value of V implies that the external force satisfies the following inequality $F > \kappa_\Gamma$. The signed distance function (SDF) can be used as the initial condition for (2.7).

Finally, using the zero Neumann boundary condition we define the following initial-boundary value problem

$$\begin{aligned} \partial_t u(t,x) &= |\nabla u|_\varepsilon \nabla \cdot \left(g^0 \frac{\nabla u}{|\nabla u|_\varepsilon}\right) - g^0 |\nabla u|_\varepsilon F && \text{in } (0,T)\times\Omega\,, \\ \frac{\partial u}{\partial n}(t,x) &= 0 && \text{on } (0,T)\times\partial\Omega\,, \\ u(0,x) &= d_{\Gamma_0}(x) && \text{in } \Omega\,. \end{aligned}$$

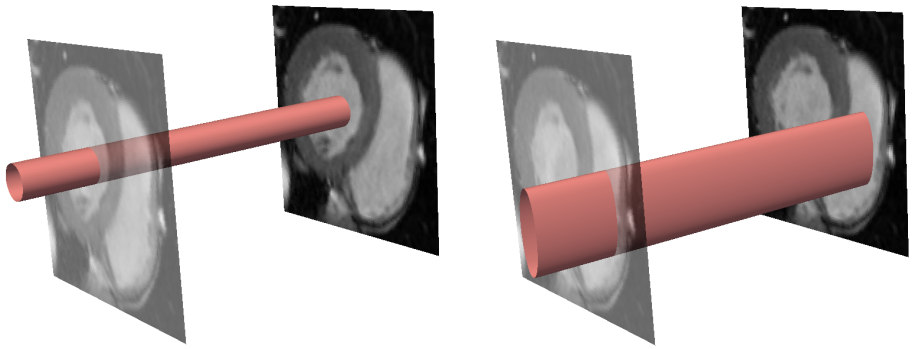

(a) (b)

Fig. 2.1: Initial segmentation surface for a segmentation of the left ventricle (a) and the right ventricle (b).

In case of 2D+t data covering the whole cardiac cycle, we can modify the boundary condition to be periodic in the time axis.

3. Numerical scheme. The initial-boundary value problem is numerically solved using the efficient and unconditionally stable semi-implicit time discretization and the three-dimensional co-volume spatial discretization introduced in [7], [9].

For the time discretization of the nonlinear diffusion equation (2.7) a semi-implicit scheme is used. We choose the uniform discrete time step τ and approximate the time derivative in (2.7) by the backward difference. The linear terms of the equation are approximated at the current time level while the nonlinear terms (i.e. $|\nabla u|_\varepsilon$) are treated at the previous time level. In this way we obtain the following semi-implicit discretization

$$\frac{1}{|\nabla u^{k-1}|_\varepsilon}\frac{u^k - u^{k-1}}{\tau} = \nabla \cdot \left(g^0 \frac{\nabla u^k}{|\nabla u^{k-1}|_\varepsilon} \right) - g^0 F \,. \tag{3.1}$$

For a spatial discretization of (2.7) a co-volume numerical scheme is applied. The co-volume method is used to construct a fully-discrete system of equations. A 3D digital image is recorded on a structure of voxels with the cubic shape. Each voxel includes the values of I^0 influencing the segmentation model. The spatial approximations of the segmentation function u is related to the voxel centers.

The gradient of the segmentation function has to be evaluated at the previous time step ($|\nabla u^{k-1}|_\varepsilon$) in (3.1). To that goal the 3D tetrahedral grid is put into the voxel structure and a piecewise linear representation of the segmentation function on such a grid is applied. This approach provides the constant value of the gradient in tetrahedra allowing the simple and fast construction of a fully-discrete system of equations. The tetrahedral grid is build using following construction. Each cubic voxel is divided into 6 pyramids with a vertex given by the voxel center and base surfaces given by the voxel boundary faces (see Fig. 3.1a). Then the neighbouring pyramids of the neighbouring voxels are joined together to form an octahedron (Fig. 3.1b). These octahedra are split into 4 tetrahedra using diagonals of the voxel boundary face (see

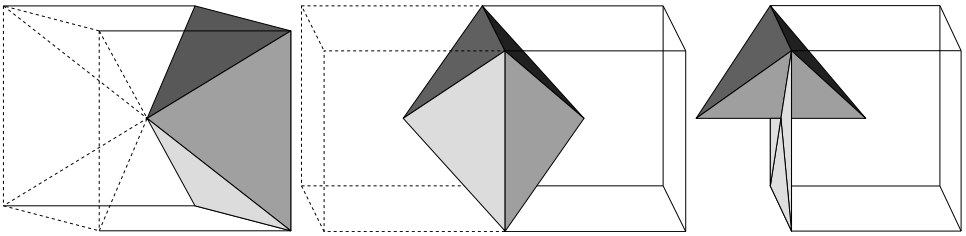

Fig. 3.1: Construction of the tetrahedral grid: (a) splitting of voxel into 6 pyramids, (b) joining of neighbouring pyramids of neighbouring voxels, (c) splitting of joined pyramides into 4 octahedra.

Fig. 3.1c). From this approach follows that the voxel center is a common vertex of 24 tetrahedra.

Here we mention the co-volume spatial discretization briefly. To see a detailed formulation of this scheme please follow the references cited below. Roughly speaking, the co-volume discretization is mainly based on the construction of two meshes. First, the primary mesh built of 3D tetrahedra mentioned in previous paragraph and the complementary mesh which corresponds to the voxel structure. As it is usual in the finite volume method, we integrate (3.1) over each co-volume p. We obtain

$$\int_p \frac{1}{|\nabla u^{k-1}|_\varepsilon} \frac{u^k - u^{k-1}}{\tau} \,\mathrm{d}x = \int_p \nabla \cdot \left(g^0 \frac{\nabla u^k}{|\nabla u^{k-1}|_\varepsilon} \right) \,\mathrm{d}x - \int_p g^0 F \,\mathrm{d}x \,. \tag{3.2}$$

The approximation of the left-hand side and the first term on the right-hand side of (3.2) can be found in [7], [9]. Hence we provide the result of the approximation only for the second term on the right-hand side of (3.2) in the form

$$\int_p g^0 F \,\mathrm{d}x \approx m(p) g_p^0 F \,, \tag{3.3}$$

where g_p^0 denotes an approximation of g^0 on the co-volume p and $m(p)$ is the measure of p in $\mathbb{R}^3$, e.g. for a regular cubic co-volume mesh we have $m(p) = h^3$, where h denotes an edge length of a cube. The evaluation of g_p^0 can be done in following way. We solve numerically the linear heat equation for time t corresponding to the variance σ^2, i.e. $t = \sigma^2/2$, with the initial condition given by I^0. Then we may construct its piecewise linear representation on the grid and get a constant value of g^0 on every tetrahedron. Let $G_p^{0,i}, i = 1, \ldots, 24$ denote the approximation of the gradient on each tetrahedron corresponding to the center of co-volume p (see [15]). Then we use following approximation of g_0 on p

$$g_p^0 \approx g \left(\frac{1}{24} \sum_{i=1}^{24} G_p^{0,i} \right) . \tag{3.4}$$

As mentioned above, this discretization leads to a linear system of equations, which has to be solved at each time step. For this purpose the SOR (Successive

Over-Relaxation) iterative method is used. The solution of the linear system is improved by a parallel method using message passing interface (MPI) standard. For the parallelization of the algorithm the parallel version (Red-Black SOR method) of SOR method is implemented (see [7], [15]). A similar scheme implemented on GPU using the CUDA toolkit can be found in [19].

3.1. Parameter setting. In this section we explain how the computational parameters for the segmentation of the left/right heart ventricle from CMR data by means of (2.7) are set up.

The parameter ε provides the regularization of the denominator in (2.4). The convergence rate of the SOR method depends on this parameter – a lower value of ε slows down the convergence. The value $\varepsilon = 10^{-3}$ is a suitable compromise. The spatial step is given as $h = 1/(\max\{n_x, n_y, n_z\} - 1)$, the time step τ equals 10^{-3}.

The parameters λ and $\sigma_{x,y,z}$ are included in the edge detector g^0 defined in Section 2. The parameter σ characterizes the variance of Gaussian smoothing kernel which is responsible for the presmoothing of the input data. The sensitivity of the edge detector depends on value of the parameter λ. Very low values of λ decrease the efficiency of the edge detection. On the other hand, very high values of λ can cause the detection of spurious edges (i.e. noise, blood flow artifacts, etc.). These two parameters are dependent each of other. Higher values of $\sigma_{x,y,z}$ require higher values of λ and vice versa. In our algorithm, we set $\sigma_{x,y} = 2h, \sigma_z = \sigma_x n_z/n_x$ (our CMR data holds $n_x = n_y, n_z < n_x$) and $\lambda = 15$.

Finally, we have to specify the external force parameter included in the equation (2.1). Satisfying the condition $F > \kappa_\Gamma$, we use $F = 50$.

3.2. Stopping criterion. Here the problem of successful termination of the segmentation process is discussed. There are several possibilities to stop the segmentation process. The simplest criterion could be to stop the process after the prescribed number of iterations. This could be a good criterion for known input data only (we know the stopping time before we start the process). Better possibility is to use an automated stopping criterion. Typically the computation is stopped as soon as the following inequality holds (see [27]):

$$\frac{1}{M}\sum_{i,j,l}\left|u^k_{i,j,l} - u^{k-1}_{i,j,l}\right| \le C\tau h^2\,, \tag{3.5}$$

where the sum is over all grid points, $M = n_x n_y n_z$ and C is a constant. As we can see from (3.5) this criterion is time and memory consuming because of storing u^{k-1}. At the same time (3.5) is too strict for our computation. It would be enough to consider the changes in the segmentation surface only (the zero level set of u).

In our algorithm we use the following automated stopping criterion

$$\sum_{i=0}^{N_0-1} D(u^{k-i}) \le K\,, \tag{3.6}$$

where $D(u^k)$ denotes the difference in the number of voxels inside the segmentation volume between two time steps k and $k-1$, i.e. $D(u^k) = \left|S(u^k) - S(u^{k-1})\right|$, where $S(u^k)$ denotes the number of voxels inside the segmentation volume, i.e. the number of grid points for which $u^k_{i,j} \le 0$. The criterion (3.6) claims that the process is stopped after k time iterations if $D(u^k) + D(u^{k-1}) + \ldots + D(u^{k-N_0+1}) \le K$ holds, i.e. the

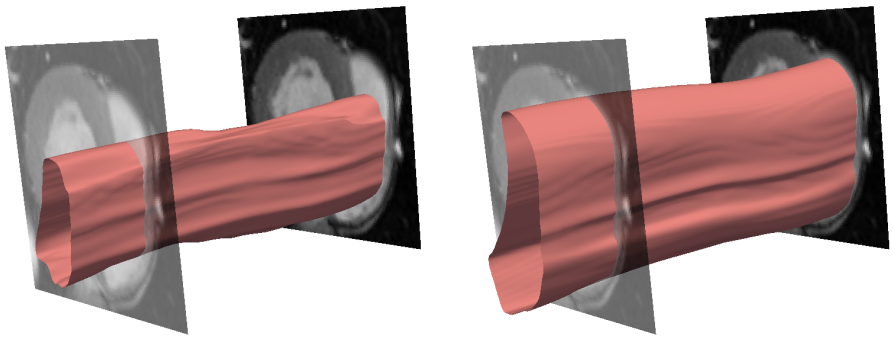

(a) (b)

Fig. 4.1: Right ventricle segmentation: (a) segmentation surface after 20 time iterations , (b) final shape of segmentation surface after 200 time iterations.

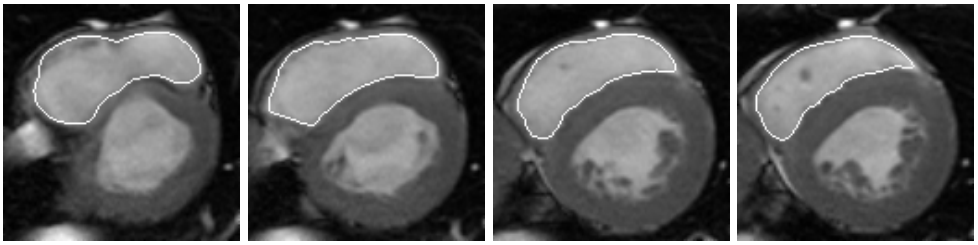

Fig. 4.2: Right ventricle segmentation: Result of the segmentation depicted for time frame T24 and slices S01–S04. White line corresponds to the segmentation surface at given time frame.

changing of segmentation volume (segmentation surface) slows down enough. In our experience good results are achieved using $N_0 = 3$ and $K = 100$.

4. Numerical results. Given the extent of this contribution, the data for a single patient are chosen as an example of the segmentation results. The size of CMR data for this patient equals $128 \times 128 \times 26 \times 12$. The images for selected slices and time frames are depicted in Figures 1.1 and 1.2. As we mentioned in Section 2.1 the initial condition has to be manually placed inside the left/heart ventricle. In Figure 2.1a we can see an initial cylinder placed into the left ventricle, whereas in Figure 2.1b the initial elliptic cylinder is placed into the right ventricle.

The result of the right ventricle segmentation for the slice S02 is depicted in Fig. 4.1. In Fig. 4.1a we can see the shape of a segmentation surface after 20 time iteration. Stopping criterion (3.6) terminated the segmentation process after 200 time iteration; Fig. 4.1b presents the result of segmentation process. As we can see in Fig. 1.1 the right ventricle is well visible only for slices S01–S04. Therefore, we can perform the segmentation for these slices and get the results depicted in Fig. 4.2.

In the same way the results of the left ventricle segmentation are shown. The

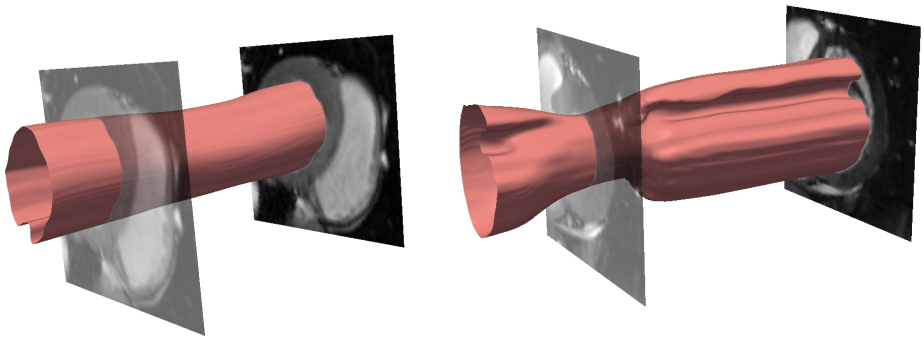

(a) (b)

Fig. 4.3: Left ventricle segmentation: (a) result of segmentation for the patient (250 time iterations), (b) final shape of segmentation surface for the healthy volunteer after 300 time iterations (data size: $128 \times 128 \times 80 \times 1$).

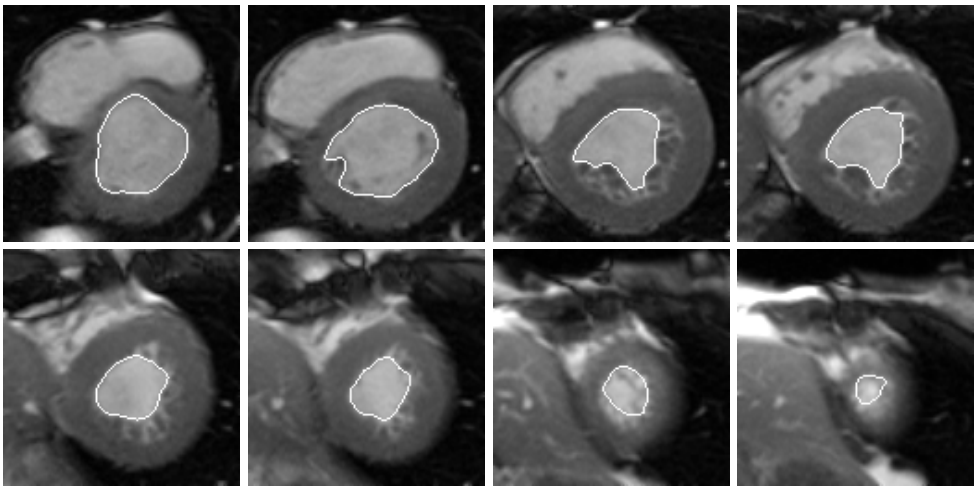

Fig. 4.4: Left ventricle segmentation: Result of the segmentation depicted for time frame T01 and slices S01, S02, S04, S05, S07, S08, S10, S11. White line corresponds to the segmentation surface at given time frame

final shape of the segmentation surface for the slice S02 after 250 time iteration is contained in Fig. 4.3a. The investigated patient has low contractility of myocardium. In order to see the difference between the shapes of final segmentation surfaces for hearts with low and high contractility we apply our algorithm on a healthy volunteer. The result is depicted in Fig. 4.3b which has a clearly different shape. From Fig. 1.1 it follows that we can perform the segmentation of the left ventricle for slices S01–S11 and obtain the results shown in Fig. 4.4.

Finally, we introduce the computing environment. Table 4.1 shows the computing

CPUs	2	4	8	16
time (secs)	5542.7	2820.4	1411.8	710.9
speed-up	2	3.93	7.85	15.59
efficiency	1	0.98	0.98	0.97

Table 4.1: Computing times and speed-up on 2 to 16 CPUs

CPUs	1	2	4	8	16
Time (secs)	6095.9	5542.7	2820.4	1411.8	710.9
Speed-up	1	1.09	2.16	4.32	8.57
Efficiency	1	0.55	0.54	0.54	0.54

Table 4.2: Computing times and speed-up on 1 to 16 CPUs

times in second after 20 iterations are performed. As we can see that the efficiency as well as the speed-up is high using larger number of processors. This result is surprising and requires further discussion. Table 4.2 represents the comparison to the computating using serial code (serial version of SOR method).

5. Conclusion. In the presented paper we apply the segmentation algorithm based on the level set equation to the problem of CMR data segmentation. The algorithm is based on the numerical scheme using the semi-implicit discretization in time and the co-volume method in space. The algorithm was tested on and applied to the real CMR data. The data were provided by the Institute for Clinical and Experimental Medicine in Prague[1]. We presented the segmentation results both for a patient and a healthy volunteer with satisfactory results. Compared to the 2D approach based on similar mathematical model introduced in [12] the 2D+t model provides time continuity in segmented data and higher accuracy of the heart ventricle volume estimation. Moreover, the results of the right heart ventricle segmentation using the 2D+t approach are more accurate than the results using the 2D segmentation model.

Acknowledgements. This work was supported by the grant of the Ministry of Education of the Czech Republic MSM6840770010 "Applied Mathematics in Technical and Physical Sciences", by the project "Advanced Supercomputing Methods for Implementation of Mathematical Models" of the Student Grant Agency of the Czech Technical University in Prague No. SGS11/161/OHK4/3T/14 and the HPC-EUROPA2 project (project number: 228398) with the support of the European Commission – Capacities Area – Research Infrastructures.

REFERENCES

[1] Beneš, M., Chalupecký, V., Mikula, K.: Geometrical image segmentation by the Allen-Cahn equation, *Applied Numerical Mathematics 51*, 187–205 (2004)

[2] Beneš, M., Kimura, M., Pauš, P. and Ševčovič, D., Tsujikawa, T., Yazaki, Sh.: Application of a Curvature Adjusted Method in Image Segmentation, *Bulletin of the Institute of Mathematics*, Academia Sinica (New Series) 2008, 509–523 (2008)

[1] IKEM Praha, `http://www.ikem.cz/www/en`

[3] Bogaert, J., Dymarkowski, S., Taylor, A. M.: Clinical cardiac MRI, *Springer-Verlag*, Berlin Heidelberg, (2005)
[4] Cao, F.: Geometric Curve Evolution and Image Processing, *Lecture Notes in Mathematics*, No 1805, Springer Verlag, Février (2003)
[5] Caselles, V., Kimmel, R., Sapiro, G.: Geodesic active contours, *International Journal of Computer Vision*, Vol. 22, 61–79, (1997)
[6] Chabiniok, R.: Personalized Biomechanical Heart Modeling for Clinical Applications, *Université Pierre et Marie Curie - Paris 6*, PhD thesis, 2011
[7] Corsaro, S., Mikula, K., Sarti, A., Sgallari, F.: Semi-implicit co-volume method in 3D image segmentation, *SIAM Journal on Scientific Computing, Vol. 28*, No. 6 (2006), 2248–2265
[8] Evans, L. C., and Spruck, J.: Motion of level sets by mean curvature I, *J. Diff. Geom.*, Vol. 33, 381–635 (1991)
[9] Handlovičová, A., Mikula, K., Sgallari, F.: Semi-implicit complementary volume scheme for solving level set like equations in image processing and curve evolution, *Numerische Mathematik, Vol. 93*, No. 4, 675–695 (2003)
[10] Loucký J., Oberhuber T.: Graph cuts in segmentation of a left ventricle from MRI data, *Proceedings of Czech-Japanese Seminar in Applied Mathematics 2010, COE Lecture Note, 2012*, vol. 36, 46–54
[11] Lynch, M., Ghita, O., Whelan, P. F.: Segmentation of the Left Ventricle of the Heart in 3D+t MRI Data Using an Optimized Non-Rigid Temporal Model, *IEEE Transactions on Medical Imaging 27(2)*, 195–203 (2008)
[12] Máca R., Beneš M., Tintěra J.: Application of a degenerate diffusion method in medical image processing, *Journal of Math-for-Industry*, Kyushu University, Fukuoka, Vol. 3 (2011C-5), 33–40
[13] Mikula, K.: Numerical solution, analysis and application of geometrical nonlinear diffusion equations, *Edition of Scientific Publications*, No. 34, Publishing House of the Slovak University of Technology, Bratislava (2006)
[14] Mikula, K., Preusser, T., Rumpf, M.: Morphological image sequence processing, *Computing and Visualization in Science*, Vol. 6, No. 4, 197–209 (2004)
[15] Mikula, K., Sarti, A.: Parallel co-volume subjective surface method for 3D medical image segmentation, *Parametric and Geometric Deformable Models: An application in Biomaterials and Medical Imagery*, Volume-II, Springer Publishers, (Eds. Jasjit S. Suri and Aly Farag), 123–160 (2007)
[16] Mikula, K., Sarti, A., Sgallari, F.: Co-Volume Level Set Method in Subjective Surface Based Medical Image Segmentation, *Handbook of Biomedical Image Analysis*, Springer US, 583–626 (2005)
[17] Montagnat, J., Delingette, H.: 4D deformable models with temporal constraints: application to 4D cardiac image segmentation, *in Medical Image Analysis (MedIA)*, Vol. 9 (1), 87–100 (2005)
[18] Oberhuber T.: Complementary finite volume scheme for the anisotropic surface diffusion flow *Proceedings of Algoritmy 2009, Handlovičová A., Frolkovič P., Mikula K. and Ševčovič D. (ed.)*, 153–164 (2009)
[19] Oberhuber T., Suzuki A., Žabka V.: The CUDA implementation of the method of lines for the curvature dependent flows, *Kybernetika*, Vol. 47(2), 251–272 (2011)
[20] Osher, S., Fedkiw, R.: Level Set Methods and Dynamic Implicit Surfaces, *Springer Verlag*, (2003)
[21] Paragios, N.: Variational Methods and Partial Differential Equations in Cardiac Image Analysis, *Invited Publication : IEEE International Symposium on Biomedical Imaging: From Nano to Macro*, (2004)
[22] Perona, P., Malk, J.: Scale space and edge detection using anisotropic diffusion, *Proc. IEEE Computer Society Workshop on Computer Vision*, (1987)
[23] Sapiro, G.: Geometric Partial Differential Equations and Image Processing, *Cambridge University Press*, (2001)
[24] Sarti, A., Malladi, R., Sethian, J.A.: Subjective Surfaces: A Geometric Model for Boundary Completion, *International Journal of Computer Vision*, Vol. 46, No. 3, 201–221 (2002)
[25] Sarti, A., Mikula, K., Sgallari, F.: Nonlinear multiscale analysis of 3D echocardiographic sequences, *IEEE Transactions on Medical Imaging*, Vol. 18, No.6, 453–467 (1999)
[26] Sethian, J. A.: Level Set Methods, *Cambridge University Press*, (1996)
[27] Zhao, H. K., Osher, S., Chan, T., Merriman, B.: A variational level set approach to multiphase motion, *J. Comput. Phys. 127*, 179–195 (1996)